

Coherent polariton dynamics in coupled highly-dissipative cavity quantum electrodynamics

Yong-Chun Liu^{1,2}, Xingsheng Luan², Hao-Kun Li¹, Qihuang Gong¹, Chee Wei Wong^{2,*} and Yun-Feng Xiao^{1,†}

¹State Key Laboratory for Mesoscopic Physics and School of Physics,

Peking University; Collaborative Innovation Center of Quantum Matter, Beijing 100871, P. R. China and

²Optical Nanostructures Laboratory, Columbia University, New York, NY 10027, USA

(Dated: September 6, 2018)

Coherent light-matter interaction at the single photon and electronic qubit level promises the remarkable potential for nonclassical information processing. Against the efforts of improving the figure of merit of the cavities, here we demonstrate strong anharmonicity in the polariton dressed states via dark state resonances in a highly dissipative cavity. It is shown that vacuum Rabi oscillation occurs for a single quantum emitter inside a cavity even with bosonic decay-to-interaction rate ratio exceeding 10^2 , when the photon field is coupled to an auxiliary high- Q cavity. Moreover, photon blockade is observable in such a highly-dissipative cavity quantum electrodynamics system. This study provides a promising platform for overcoming decoherence and advancing the coherent manipulation of polariton qubits.

PACS numbers: 42.50.Pq, 42.50.Ct

Cavity quantum electrodynamics (QED) (for a review, see [1]) provides a critical resource for quantum information processing [2–12]. For coherent manipulation, a key prerequisite is to reach the strong coupling regime, where the emitter-field coupling strength exceeds the decay rates of the emitter and the cavity field. In the past two decades great efforts have been made to improve the quality (Q) factor and reduce the mode volume (V) of the resonators for stronger interactions, using Fabry-Pérot cavities [13, 14], Bragg cavities [15–17], whispering-gallery mode cavities [18–23], photonic crystal cavities [24–30], hybrid plasmonic-photonic cavities [31] and transmission-line microwave cavities [32], along with theoretical studies of coupled-cavity QED through a waveguide [33–36]. However, it remains difficult to achieve high Q and small V simultaneously for the same-type resonator. Fundamentally, this is related to the diffraction limit. A smaller V corresponds to a larger radiative decay rate and more significant roughness scattering, leading to a lower Q . Different-type resonators possess their own unique properties, but the trade-off between high Q and small V still exists. For example, whispering-gallery mode cavities possess ultrahigh Q factors, while the mode volumes are relatively large; for photonic crystal cavities, sub-wavelength light confinement can be realized whereas the Q factors are relatively low.

Unlike the efforts to improve the Q/\sqrt{V} figure of merit of the cavities, here we propose to reach the strong coupling regime via dark state resonances, which removes the requirement for high Q and small V for the same cavity. By coupling the originally weak-coupled cavity QED system with high cavity dissipation to an auxiliary cavity mode with high- Q but large V , a strong dark state interaction takes place. We demonstrate that vacuum Rabi oscillations and anharmonicity in the polariton dressed states occur even when the cavity decay rate is

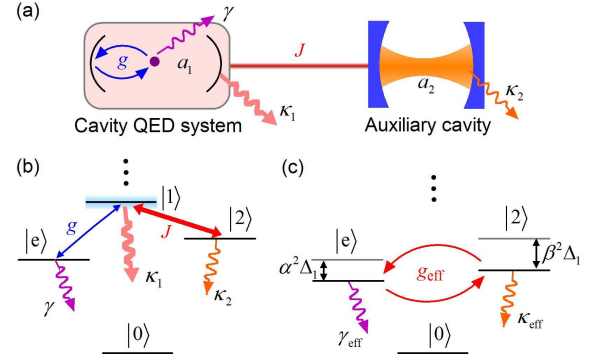


FIG. 1. (color online) (a) Schematic of the cavity QED system coupled to an auxiliary cavity. (b) Energy level diagram of the coupled system. The lowest four energy levels are plotted, including the ground state $|0\rangle$, the first excited state triplets $|e\rangle$, $|1\rangle$ and $|2\rangle$, which denote the states $|g\rangle|0\rangle_1|0\rangle_2$, $|e\rangle|0\rangle_1|0\rangle_2$, $|g\rangle|1\rangle_1|0\rangle_2$ and $|g\rangle|0\rangle_1|1\rangle_2$. (c) Sketch of the dark state interaction after eliminating state $|1\rangle$.

two orders of magnitude larger than the interaction rate.

As shown in Fig. 1(a), a cavity QED system, consisting of a dipole quantum emitter and a cavity, is coupled to an auxiliary cavity through a short-length single-mode waveguide. Here we take Fabry-Pérot cavity QED system as an example, while it allows generalization to other physical implementations, including solid-state circuit QED systems. In the frame rotating at the emitter's resonance frequency ω_e , the system Hamiltonian reads $H = \Delta_1 a_1^\dagger a_1 + \Delta_2 a_2^\dagger a_2 + g(a_1^\dagger \sigma_- + a_1 \sigma_+) + J(a_1^\dagger a_2 + a_2^\dagger a_1)$, where a_1 , a_2 are the annihilation operators of the two cavity modes; $\sigma_- \equiv |g\rangle\langle e| = \sigma_+^\dagger$ stands for the descending operator of the emitter with $|g\rangle$ ($|e\rangle$) being the ground (excited) state; $\Delta_1 \equiv \omega_1 - \omega_e$ and $\Delta_2 \equiv \omega_2 - \omega_e$ represent the detunings with ω_1 (ω_2) being the resonance frequency of mode a_1 (a_2); g denotes the emitter-

field coupling strength between the emitter and mode a_1 ; J describes the inter-cavity coupling strength between mode a_1 and a_2 [37–39]. Without loss of generality, we have assumed g and J to be real numbers. Taking the dissipations into consideration, the system is described by the quantum master equation $\dot{\rho} = i[\rho, H] + \kappa_1 \mathcal{D}[a_1]\rho + \kappa_2 \mathcal{D}[a_2]\rho + \gamma \mathcal{D}[\sigma_-]\rho$, where $\mathcal{D}[\hat{o}]\rho = \hat{o}\rho\hat{o}^\dagger - (\hat{o}^\dagger\hat{o}\rho + \rho\hat{o}^\dagger\hat{o})/2$ is the standard dissipator in Lindblad form; κ_1 , κ_2 and γ represent the decay rates of modes a_1 , a_2 and the emitter.

We show how highly dissipative cavity QED systems ($\kappa_1 \gg g$) can be turned into the effective strong coupling regime via dark state interaction. By eliminating mode a_1 , we obtain the effective interaction between the emitter and the auxiliary cavity mode a_2 , with the effective Hamiltonian

$$H_{\text{eff}} = (\Delta_2 - \beta^2 \Delta_1) a_2^\dagger a_2 - \frac{1}{2} \alpha^2 \Delta_1 \sigma_z + g_{\text{eff}} (a_2^\dagger \sigma_- + a_2 \sigma_+), \quad (1)$$

where $\sigma_z \equiv |e\rangle\langle e| - |g\rangle\langle g|$, α and β represent the scaled dimensionless interaction parameters given by $\alpha = g/(\Delta_1^2 + \kappa_1^2/4)^{1/2}$ and $\beta = J/(\Delta_1^2 + \kappa_2^2/4)^{1/2}$, respectively. The effective coupling strength, detuning, decay rates of the cavity field and the emitter are described by

$$\begin{aligned} g_{\text{eff}} &= \beta g, & \Delta_{\text{eff}} &= \Delta_2 + (\alpha^2 - \beta^2) \Delta_1, \\ \kappa_{\text{eff}} &= \kappa_2 + \beta^2 \kappa_1, & \gamma_{\text{eff}} &= \gamma + \alpha^2 \kappa_1. \end{aligned} \quad (2)$$

In Fig. 1(b) we plot the energy level diagram, which displays the lowest four energy levels of the system. It reveals that the emitter-field interaction between state $|e\rangle$ (short for $|e\rangle|0\rangle_1|0\rangle_2$) and state $|1\rangle$ (short for $|g\rangle|1\rangle_1|0\rangle_2$), together with the inter-cavity interaction between state $|2\rangle$ (short for $|g\rangle|0\rangle_1|1\rangle_2$) and state $|1\rangle$, yields the effective dark state interaction between state $|e\rangle$ and state $|2\rangle$. As shown in Eqs. (1)-(2) and illustrated in Fig. 1(c), after the the elimination of state states $|1\rangle$, the states $|e\rangle$ and $|2\rangle$ acquire energy shifts of $-\alpha^2 \Delta_1$ and $-\beta^2 \Delta_1$, together with broadenings of $\alpha^2 \kappa_1$ and $\beta^2 \kappa_1$.

Equations (2) show that the effective coupling strength g_{eff} depends linearly on β while the effective decay rates κ_{eff} and γ_{eff} are quadratic functions of β and α , respectively. As a result, for $(\alpha, \beta) \ll 1$, the effective coupling strength will be larger than the decay rates, driving the effective interaction into the strong coupling regime. In Figs. 2(a) and (b) the parameters given by Eq. (2) as functions of inter-cavity interaction strength J and the first cavity mode's detuning Δ_1 are plotted, respectively. It reveals that with a suitable J and Δ_1 , the effective coupling strength g_{eff} exceeds both decay rates κ_{eff} and γ_{eff} , even for large cavity decay rate $\kappa_1/g = 100$. As shown in the insets of Figs. 2(a) and (b), the ranges of J and Δ_1 for effective strong coupling have both lower and upper bounds. To gain more insights on the parameter ranges, in Figs. 2(c)-(e) we plot $g_{\text{eff}}/\kappa_{\text{eff}}$, $g_{\text{eff}}/\gamma_{\text{eff}}$ and the cooperativity parameter $C_{\text{eff}} \equiv g_{\text{eff}}^2/(\kappa_{\text{eff}}\gamma_{\text{eff}})$ as

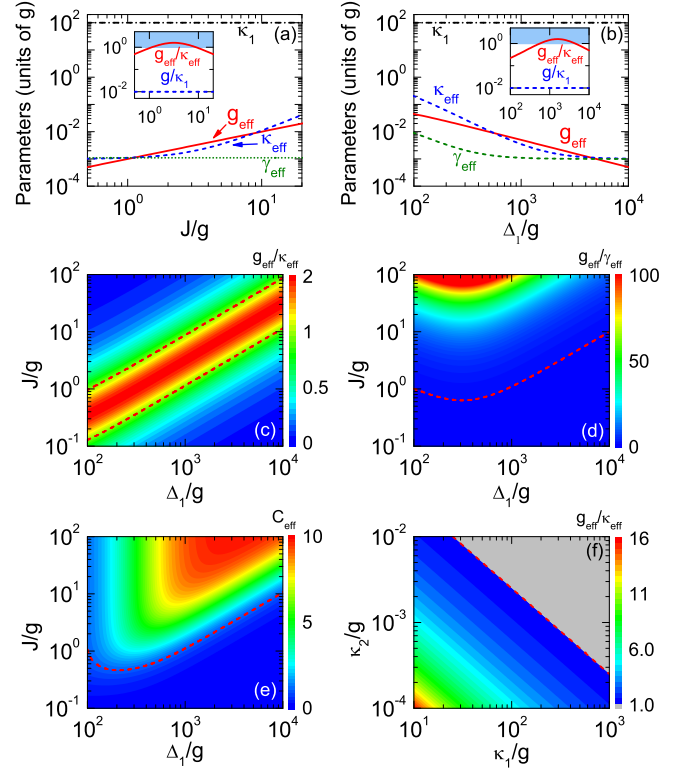


FIG. 2. (color online) Parameters κ_1 (black dashed-dotted curves), g_{eff} (red solid curves), κ_{eff} (blue dashed curves) and γ_{eff} (green dotted curves) as functions of inter-cavity interaction strength (a) and the first cavity mode's detuning (b). Both the horizontal and vertical axes are in the units of the emitter-field coupling strength g . The insets in (a) and (b) show $g_{\text{eff}}/\kappa_{\text{eff}}$ (red solid curves) and $g_{\text{eff}}/\gamma_{\text{eff}}$ (blue dashed curves); the blue shaded regions indicate $g_{\text{eff}}/\kappa_{\text{eff}} > 1$. (c)-(e): Contour plots of $g_{\text{eff}}/\kappa_{\text{eff}}$, $g_{\text{eff}}/\gamma_{\text{eff}}$ and the cooperativity C_{eff} as functions of Δ_1/g and J/g ; the red dashed curves denote the contour value of 1. In (a), $\Delta_1/\kappa_1 = 10$; in (b), $J/g = 5$; in (a)-(e), $\kappa_1/g = 100$, $\kappa_2/g = 10^{-3}$, $\gamma/g = 10^{-3}$ and $\Delta_2 = (\beta^2 - \alpha^2)\Delta_1$. (f) Contour plot of $g_{\text{eff}}/\kappa_{\text{eff}}$ as functions of κ_1/g and κ_2/g for $\beta = \sqrt{\kappa_2/\kappa_1}$; the red dashed curve denotes $\kappa_2 = g^2/(4\kappa_1)$.

functions of Δ_1 and J . It reveals that a large Δ_1 and a corresponding large J lead the system deeply into the effective strong coupling regime. Examining Eq. (2), for $J > g > \kappa_2 \sim \gamma$, it gives $\kappa_{\text{eff}} > \gamma_{\text{eff}}$ with negligible γ_{eff} . In this case, the maximum effective coupling-to-decay rate ratio reads $g_{\text{eff}}/\kappa_{\text{eff}} = g/(2\sqrt{\kappa_1\kappa_2})$, obtained when $\beta = \sqrt{\kappa_2/\kappa_1}$. Thus the strong coupling condition $g_{\text{eff}} > \kappa_{\text{eff}}$ can be fulfilled when $\kappa_2 < g^2/(4\kappa_1)$. This is verified by the contour plot in Fig. 2(f), which displays $g_{\text{eff}}/\kappa_{\text{eff}}$ as a function of κ_1 and κ_2 . The bottom left region indicates the strong effective coupling parameter regime, with g_{eff} in excess of κ_{eff} by more than one order of magnitude.

To demonstrate that the effective parameters in Eq. (2) exactly describe the physical interaction, we diago-

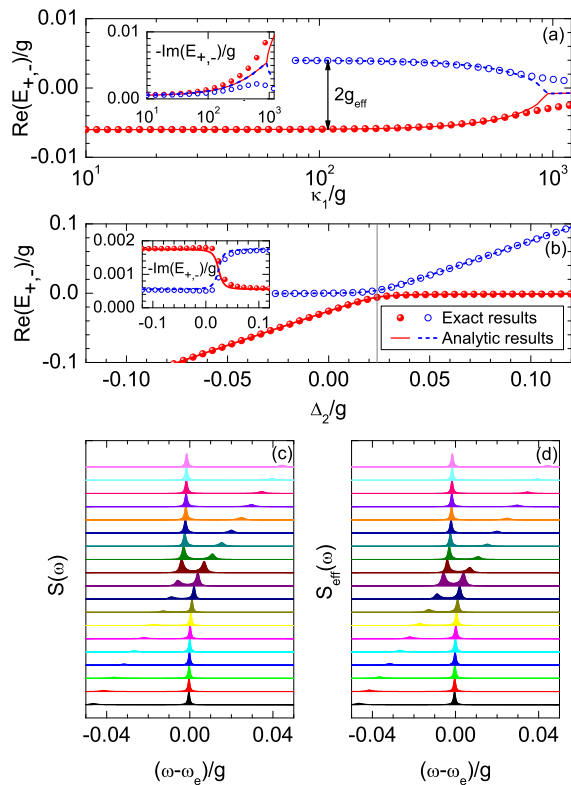


FIG. 3. (color online) (a) and (b): Eigenvalues E_{\pm} for states $|0\rangle_1|1, \pm\rangle_{e2}$ as functions of κ_1/g and Δ_2/g . The main figures and the insets show the real and imaginary parts of the eigenvalues, respectively. The circles correspond to the exact results and the curves denote the results obtained from the effective Hamiltonian and effective parameters [Eqs. (1)-(2)]. The gray vertical line in (b) denotes $\Delta_2 = (\beta^2 - \alpha^2)\Delta_1$. (c) and (d): Normalized spectra $S(\omega)$ and effective spectra $S_{\text{eff}}(\omega)$ of the emitter for various Δ_2 . From top to bottom, Δ_2 decrease from $(\beta^2 - \alpha^2)\Delta_1 - 9g_{\text{eff}}$ to $(\beta^2 - \alpha^2)\Delta_1 + 9g_{\text{eff}}$ with step g_{eff} . The common parameters are the same as Fig. 2(a)-(e).

nalize the system Hamiltonian in the subspace of the first excited states. Using the non-Hermitian Hamiltonian where the decays are taken into account, the eigenenergies and the broadenings of each states are obtained as the real and imaginary parts of the eigenvalues, respectively. For the first excited states, after the diagonalization under large detuning Δ_1 , the eigenstates read $|1\rangle_1|0\rangle_{e2} \simeq |g\rangle|1\rangle_1|0\rangle_2$, $|0\rangle_1|1, \pm\rangle_{e2} \simeq (|e\rangle|0\rangle_1|0\rangle_2 \pm |g\rangle|0\rangle_1|1\rangle_2)/\sqrt{2}$. It reveals that the states $|0\rangle_1|1, \pm\rangle_{e2}$ are *dark state doublets* with respect to the decay of mode a_1 . In Figs. 3(a) we plot the real and imaginary parts of the eigenvalues E_{\pm} for the dark state doublets $|0\rangle_1|1, \pm\rangle_{e2}$ as functions of κ_1/g , where the real (imaginary) parts represent the eigenenergies (linewidths) of the states. It shows that the eigenenergies of the two states are split by $2g_{\text{eff}} = 0.01g$, and the linewidths are much smaller than the energy splitting (inset), even for κ_1/g exceeding 100. Note that the global energy shift of $0.001g (= -\alpha^2\Delta_1)$

can be eliminated by applying a unitary transformation to the effective Hamiltonian [Eq. (1)]. The results obtained from the effective Hamiltonian and effective parameters [Eqs. (1) and (2)] are in good accordance with the exact results for both the real and imaginary parts of the eigenvalues. For $\kappa_1/g \gtrsim 800$, discrepancy occurs because $\Delta_1 \gg \kappa_1$ is not satisfied.

In Fig. 3(b) we plot the eigenenergies and linewidths for states $|0\rangle_1|1, \pm\rangle_{e2}$ as functions of the detuning between mode a_2 and the emitter (Δ_2/g). Prominent avoided crossing phenomenon occurs for the eigenenergies, which occurs for the effective resonant case $\Delta_{\text{eff}} = 0$ (gray vertical line). Near the avoided crossing point the linewidths of the two polariton states are averaged compared with the large Δ_{eff} case (inset), and are swapped for increasing detuning as indication of the quantum strong coupling. The avoided crossing is further examined in Fig. 3(c), which shows the emitter's spectra $S(\omega)$ for various detunings Δ_2 through the weak excitation of mode a_2 . It shows close agreement with the effective spectra $S_{\text{eff}}(\omega)$ obtained from the effective interaction [Fig. 3(d)].

In the time domain, vacuum Rabi oscillation is a direct evidence of the coherent energy exchange between the emitter and the cavity photon field. Here we numerically solve the quantum master equation to obtain the exact results. We assume initially the emitter is in the excited state and the two cavity modes are in their vacuum states, then we obtain the exact numerical results for the time evolution of the mean photon numbers $N_1(t) = \langle a_1^\dagger a_1 \rangle$, $N_2(t) = \langle a_2^\dagger a_2 \rangle$ and the probability for the emitter being in the excited state $P_e(t) = (\langle \sigma_z \rangle + 1)/2$. As shown in Fig. 4(a), even for $\kappa_1/g = 100$, vacuum Rabi oscillation phenomenon occurs for several periods, revealing that the decoherence time is much longer than the energy exchange period. This is in contrary to the case without the auxiliary cavity as shown in the left inset of Fig. 4(a), where the emitter exponentially decays from the excited state. Note that the occupancy in mode a_1 oscillates with the maximum photon number below 10^{-5} as shown in the right inset of Fig. 4(a)], while the occupancy in mode a_2 oscillates with the maximum photon number exceeding 0.5. This reveals that the interaction is mainly between the emitter and mode a_2 , while mode a_1 is only virtually excited. The analytical results for the emitter's occupancy in the excited state, obtained from the effective parameters [Eq. (2)], is described by

$$P_e^{\text{eff}}(t) = \exp\left(-\frac{\kappa_{\text{eff}} + \gamma_{\text{eff}}}{2}t\right) \cos^2(g_{\text{eff}}t). \quad (3)$$

With vacuum Rabi frequencies $\Omega_R = 2g_{\text{eff}}$ and the decay rates $(\kappa_{\text{eff}} + \gamma_{\text{eff}})/2$, the results in the effective dark state picture (red solid curve) are in good accordance with the exact numerical results (red closed circles).

The effective strong coupling offers great potential for single-photon manipulation and quantum logic gate op-

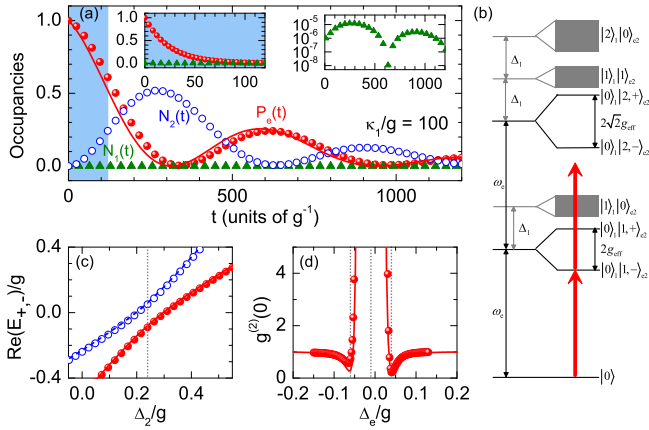


FIG. 4. (color online) (a) Time evolution of the mean photon numbers $N_1(t)$ (green triangles), $N_2(t)$ (blue open circles) and the probability for the emitter being in the excited state $P_e(t)$ (red closed circle) for $\kappa_1/g = 100$. The red solid curves correspond to the analytical results of $P_e^{\text{eff}}(t)$ [Eq. (3)]. Left inset: Comparative $N_1(t)$ (green triangles) and $P_e(t)$ (red closed circles) without the auxiliary cavity ($J = 0$) and for $\Delta_1 = 0$; the range of the horizontal axis is the same as the shaded region of the main figure. Right inset: Log scale plot of $N_1(t)$. (b) Energy level diagram of the ground state, the first and second excited states for interpretation of the photon blockade effect. (c) Eigenenergies of the second excited states $|0\rangle_1|2, \pm\rangle_{e_2}$ as functions of Δ_2/g for $\kappa_1/g = 10$. The gray vertical line denotes $\Delta_2 = (\beta^2 - \alpha^2)\Delta_1$. (d) Second-order correlation function $g^{(2)}(0)$ as a function of the probe-emitter detuning Δ_e for $\kappa_1/g = 10$. The gray vertical line denotes $\Delta_e = -\alpha^2\Delta_1 - g_{\text{eff}}$, $-\alpha^2\Delta_1$ and $-\alpha^2\Delta_1 + g_{\text{eff}}$ (from left to right). The circles correspond to the exact results and the curves indicate the results obtained from the effective Hamiltonian and effective parameters [Eqs. (1) and (2)]. The common parameters are the same as Fig. 2(a)-(e).

eration. For example, photon blockade phenomenon [40, 41] occurs in this coupled system, as illustrated in Fig. 4(b), where the energy spectrum for the ground state, the first and second excited states are plotted. The first excited state has triplet sub-levels, and the second excited state has quintet sub-levels including $|0\rangle_1|2, \pm\rangle_{e_2}$, $|1\rangle_1|1, \pm\rangle_{e_2}$ and $|2\rangle_1|0\rangle_{e_2}$. The computed energy levels $|0\rangle_1|2, \pm\rangle_{e_2}$ are shown in Fig. 4(c), which are dark state doublets with energy splitting of $2\sqrt{2}g_{\text{eff}}$ at the minimal avoided crossing point. Due to the strong anharmonicity of the level spacing between the polariton dressed states, photon blockade of the second photon by the first photon can occur. This is quantitatively characterized by the zero-delay second-order correlation function $g^{(2)}(0) \equiv \lim_{t \rightarrow \infty} \langle a_2^\dagger a_2^\dagger a_2 a_2 \rangle(t) / \langle a_2^\dagger a_2 \rangle^2(t)$. We use a weak probe laser input with frequency ω to obtain the exact results of $g^{(2)}(0)$ numerically. In Fig. 4(d) $g^{(2)}(0)$ as a function of the probe-emitter detuning $\Delta_e \equiv \omega - \omega_e$ is plotted. It reveals that $g^{(2)}(0)$ approaches 0 for $\Delta_e = -\alpha^2\Delta_1 \pm g_{\text{eff}}$, indicating strong antibunching effect and sub-Poissonian photon statistics. Under such

strong coupling regime, with an external field pumping the system, it is also promising for the generation of one-atom lasing [42–44].

It should be noted that, although the auxiliary cavity is required to be high- Q ($\kappa_2 < g$), it does not need to interact directly with the emitter, and its mode volume is not necessary to be small. Therefore, the scheme does not require a high figure of merit Q/\sqrt{V} for the auxiliary cavity. Together with the allowed low Q factor for the primary cavity, both the two cavities can be low in figure of merit Q/\sqrt{V} . This approach is also generic and can be applied to any cavity QED systems with different physical implementations, including solid-state circuit QED systems. In the viewpoint of mode density shaping [45], at the second cavity mode's resonance frequency the system's mode density is enhanced, and it leads to the effective interaction between the second cavity mode and the emitter.

In summary, we have presented a protocol for realizing effective strong coupling in a highly-dissipative cavity QED system. By employing the coupled cavity configuration, we show that a highly dissipative cavity interacting simultaneously with a single emitter and an auxiliary cavity leads to the dark state resonance between the emitter and the auxiliary cavity. It is demonstrated that effective strong coupling can be achieved even with low Q/\sqrt{V} cavities, with prominent vacuum Rabi oscillation and ladder anharmonicity phenomena for photon blockade. The cavity coupled to the emitter can be highly dissipative even with the decay rate in excess of the interaction strength by two orders of magnitude. The system enables single photon manipulation like photon blockade and quantum logic gate operations. This approach offers opportunities to exploit both theoretical and experimental physics in the strong light-matter interaction regime without stringent cavity requirements.

This work was supported by the 973 program (No. 2013CB921904, No. 2013CB328704), NSFC (Nos. 11004003, 11222440, and 11121091), RFDPH (No. 20120001110068), NSF MWN and IGERT awards (DMR-1108176 and DGE-1069240). H.K.L. was supported by the National Fund for Fostering Talents of Basic Science (Grants No. J1030310 and No. J1103205)

* cww2014@columbia.edu

† Corresponding author: yfxiao@pku.edu.cn; URL: www.phy.pku.edu.cn/~yfxiao/index.html

- [1] G. Khitrova, H. M. Gibbs, M. Kira, S. W. Koch, and A. Scherer, *Nature Phys.* **2**, 81 (2006).
- [2] S.-B. Zheng and G.-C. Guo, *Phys. Rev. Lett.* **85**, 2392 (2000).
- [3] T. Pellizzari, S. A. Gardiner, J. I. Cirac, and P. Zoller, *Phys. Rev. Lett.* **75**, 3788 (1995).
- [4] J. I. Cirac, P. Zoller, H. J. Kimble, and H. Mabuchi,

- Phys. Rev. Lett. **78**, 3221 (1997).
- [5] L.-M. Duan and H. J. Kimble, Phys. Rev. Lett. **92**, 127902 (2004).
- [6] W. Yao, R.-B. Liu, and L. J. Sham, Phys. Rev. Lett. **95**, 030504 (2005).
- [7] C. Guerlin, J. Bernu, S. Deléglise, C. Sayrin, S. Gleyzes, S. Kuhr, M. Brune, J.-M. Raimond, and S. Haroche, Nature (London) **448**, 889 (2007).
- [8] C. Monroe, D. M. Meekhof, B. E. King, S. R. Jefferts, W. M. Itano, D. J. Wineland and P. Gould, Phys. Rev. Lett. **75**, 4011 (1995).
- [9] R. Bose, T. Kai, G. Solomon, and E. Waks, Appl. Phys. Lett. **100**, 231107 (2012).
- [10] E. Waks and J. Vučković, Phys. Rev. Lett. **96**, 153601 (2006).
- [11] Y.-C. Liu, Y.-F. Xiao, B.-B. Li, X.-F. Jiang, Y. Li, and Q. Gong, Phys. Rev. A **84**, 011805(R) (2011).
- [12] A. Majumdar, M. Bajcsy, and J. Vučković, Phys. Rev. A **85**, 041801(R) (2012).
- [13] R. J. Thompson, G. Rempe, and H. J. Kimble, Phys. Rev. Lett. **68**, 1132 (1992).
- [14] K. M. Birnbaum, A. Boca, R. Miller, A. D. Boozer, T. E. Northup, and H. J. Kimble, Nature (London) **436**, 87 (2005).
- [15] J. P. Reithmaier, G. Sek, A. Löffler, C. Hofmann, S. Kuhn, S. Reitzenstein, L. V. Keldysh, V. D. Kulakovskii, T. L. Reinecke, and A. Forchel, Nature (London) **432**, 197 (2004).
- [16] D. Press, S. Götzinger, S. Reitzenstein, C. Hofmann, A. Löffler, M. Kamp, A. Forchel, and Y. Yamamoto, Phys. Rev. Lett. **98**, 117402 (2007).
- [17] J. Kasprzak, S. Reitzenstein, E. A. Muljarov, C. Kistner, C. Schneider, M. Strauss, S. Höfling, A. Forchel, and W. Langbein, Nature Mater. **9**, 304 (2010).
- [18] E. Peter, P. Senellart, D. Martrou, A. Lemaître, J. Hours, J. M. Gérard, and J. Bloch, Phys. Rev. Lett. **95**, 067401 (2005).
- [19] T. Aoki, B. Dayan, E. Wilcut, W. P. Bowen, A. S. Parkins, T. J. Kippenberg, K. J. Vahala, and H. J. Kimble, Nature (London) **443**, 671 (2006).
- [20] Y.-S. Park, A. K. Cook, and H. Wang, Nano Lett. **6**, 2075 (2006).
- [21] N. Le Thomas, U. Woggon, O. Schops, M. Artemyev, M. Kazes, and U. Banin, Nano Lett. **6**, 557 (2006).
- [22] K. Srinivasan and O. Painter, Nature **450**, 862 (2007).
- [23] S. Schietinger, T. Schroder, and O. Benson, Nano Lett. **8**, 3911 (2008).
- [24] T. Yoshie, A. Scherer, J. Hendrickson, G. Khitrova, H. M. Gibbs, G. Rupper, C. Ell, O. B. Shchekin, and D. G. Deppe, Nature (London) **432**, 200 (2004).
- [25] A. Badolato, K. Hennessy, M. Atatüre, J. Dreiser, E. Hu, P. M. Petroff, A. Imamoglu, Science **308**, 1158 (2005).
- [26] K. Hennessy, A. Badolato, M. Winger, D. Gerace, M. Atatüre, S. Gulde, S. Fält, E. L. Hu, and A. Imamoglu, Nature (London) **445**, 896 (2007).
- [27] D. Englund, A. Faraon, I. Fushman, N. Stoltz, P. Petroff, and J. Vučković, Nature (London) **450**, 857 (2007).
- [28] A. Faraon, I. Fushman, D. Englund, N. Stoltz, P. Petroff, and J. Vuckovic, Nature Phys. **4**, 859 (2008).
- [29] M. Nomura, N. Kumagai, S. Iwamoto, Y. Ota, and Y. Arakawa, Nature Phys. **6**, 279 (2010).
- [30] R. Bose, D. Sridharan, H. Kim, G. S. Solomon, and E. Waks, Phys. Rev. Lett. **108**, 227402 (2012).
- [31] Y.-F. Xiao, Y.-C. Liu, B.-B. Li, Y.-L. Chen, Y. Li, and Q. Gong, Phys. Rev. A **85**, 031805(R) (2012).
- [32] A. Wallraff, D. I. Schuster, A. Blais, L. Frunzio, R.-S. Huang, J. Majer, S. Kumar, S. M. Girvin, and R. J. Schoelkopf, Nature (London) **431**, 162 (2004).
- [33] S. Hughes, Phys. Rev. Lett. **98**, 083603 (2007).
- [34] Z.-q. Yin and F.-l. Li, Phys. Rev. A **75**, 012324 (2007).
- [35] F. M. Hu, L. Zhou, T. Shi, and C. P. Sun, Phys. Rev. A **76**, 013819 (2007).
- [36] A. Majumdar, A. Rundquist, M. Bajcsy, and J. Vučković, Phys. Rev. B **86**, 045315 (2012).
- [37] Y. Sato, Y. Tanaka, J. Upham, Y. Takahashi, T. Asano, and S. Noda, Nature Photon. **6**, 56 (2012).
- [38] J. Cho, D. G. Angelakis, and S. Bose, Phys. Rev. A **78**, 022323 (2008).
- [39] Y.-F. Xiao, M. Li, Y.-C. Liu, Y. Li, X. Sun, and Q. Gong, Phys. Rev. A **82**, 065804 (2010).
- [40] K. M. Birnbaum, A. Boca, R. Miller, A. D. Boozer, T. E. Northup, and H. J. Kimble, Nature (London) **436**, 87 (2005).
- [41] C. Lang, D. Bozyigit, C. Eichler, L. Steffen, J. M. Fink, A. A. Abdumalikov, Jr., M. Baur, S. Filipp, M. P. da Silva, A. Blais, and A. Wallraff, Phys. Rev. Lett. **106**, 243601 (2011).
- [42] Y. Mu and C. M. Savage, Phys. Rev. A **46**, 5944 (1992).
- [43] E. del Valle and F. P. Laussy, Phys. Rev. A **84**, 043816 (2011).
- [44] J. McKeever, A. Boca, A. D. Boozer, J. R. Buck, and H. J. Kimble, Nature (London) **425**, 268 (2003).
- [45] M. D. Reed, B. R. Johnson, A. A. Houck, L. DiCarlo, J. M. Chow, D. I. Schuster, L. Frunzio, and R. J. Schoelkopf, Appl. Phys. Lett. **96**, 203110 (2010).